Physica B 404 (2009) 4942–4948

Contents lists available at ScienceDirect

Physica B

journal homepage: www.elsevier.com/locate/physb

# EPR identification of intrinsic and transition metal-related defects in $ZnGeP_2$ and other II–IV–$V_2$ compounds

W. Gehlhoff *, A. Hoffmann

*Institute for Solid State Physics, Technical University Berlin, Hardenbergstr. 36, D-10623 Berlin, Germany*

ARTICLE INFO

*Keywords:*
Compound semiconductor
Native defects
Transition metals
Magnetic resonance

ABSTRACT

Diluted magnetic semiconductors (DMS) that exhibit ferromagnetism at room temperature (RTFM) are central for the development of semiconductor spintronics. According to theoretical predictions transition metal (TM)-doped $A^{II}B^{IV}C_2^V$ chalcopyrite are promising compounds for such applications. In addition to other semiconductors, they also open the opportunity to combine the observed RTFM with their excellent nonlinear optical properties, resulting into a new class of device structures for nonlinear optics and spintronics applications. These ternary compound semiconductors have two metal sites A and B that can be substituted by the TMs. A site preference for TM incorporation is crucial for the possible explanation of ferromagnetism since dependent on the TM valence state holes or electrons can be released. The magnetic resonance studies of native defects and their transition energies, EPR investigations of isolated TMs on the two different cation lattice sites, on exchanged coupled pairs as well as the interaction of TMs with native defects will be critically reviewed and the experimental results obtained are compared with theoretical predictions.



## 1. Introduction

The $A^{II}B^{IV}C_2^V$ compounds (A=Zn, Cd, B=Ge, Si, C=P, As) are ternary compounds that crystallize in the tetragonal chalcopyrite structure and were studied in the last two decades mainly for their potential as nonlinear optical (NLO) materials for frequency conversion applications like infrared optical parametric oscillator (OPO) laser systems [1,2]. $ZnGeP_2$ and $CdGeAs_2$ are ideal candidates for NLO applications, because they have high nonlinear optical coefficient combined with adequate birefringence for phase matching. Native point defects play an important role in their efficiency for frequency conversion applications, because defect-induced bands reduce the output power of such devices.

The importance of the ternary pnictides became even more eminent with the discovery of room-temperature ferromagnetism (RTFM) in highly Mn-doped semiconducting $CdGeP_2$ [3], $ZnGeP_2$ [4] and other pnictides, because semiconductors that exhibit room-temperature ferromagnetism (RTFM) are central to the development of semiconductor spintronics. The existence of RTFM is also predicted for other transition metals. At variance with other semiconductors the pnictides open in addition the possibility to combine the observed RTFM with their excellent nonlinear optical properties, resulting in a new class of material for nonlinear optics and spintronics applications. However, like for other diluted magnetic semiconductors, the origin of the RTFM is still not settled and different models are discussed. A unique explanation of the microscopic origin of the detected FM in the various compounds doped with different TMs can only be accomplished by an efficient combination of various experimental techniques and current state-of-the art theoretical methods. To decide between the different theoretical predictions specifically detailed knowledge concerning the incorporation of TM in the different charge states at different lattice sites and the TM-induced local change of the free parameter $x_f$ of the chalcopyrite structure are necessary. Such data can be obtained in a unique way by magnetic resonance methods, especially by electron paramagnetic resonance (EPR) and by photo-EPR measurements. These methods particularly address the site selection of the doping atoms and their interaction with each other, with other defects both intrinsic and induced by strong TM doping and with free carriers. Photo-EPR delivers data on the position of the various charge states of the different native defects and TMs. For the ternary compounds there are two metallic sites A (group II) and B (group IV) that can be substituted by a TM ion. A site preference of TM ions to the group II or group IV site is crucial for a potential realization of FM since it depends on the valence state of the TM whether holes or electrons are released [5,6].

In this article the results obtained by magnetic resonance methods on the structure of native defects and their transition

* Corresponding author. Tel.: +49 30 314 26601; fax: +49 30 314 22569.
*E-mail address:* gehlhoff@sol.physik.tu-berlin.de (W. Gehlhoff).

0921-4526/$ - see front matter © 2009 Elsevier B.V. All rights reserved.
doi:10.1016/j.physb.2009.08.255

energies, EPR studies of isolated TMs and of exchanged coupled pairs as well as the interaction of TMs with native defects will be critically reviewed. The experimental results are compared with theoretical predictions.

## 2. Native defects

The atomistic and geometric structures of native defects have been investigated in detail only for $ZnGeP_2$, $ZnSiP_2$, and $CdGeAs_2$ so far. Five different native defects have been identified for $ZnGeP_2$ using EPR, ENDOR, and optically activated EPR [7–13]. High-quality single crystals optimized for the nonlinear optical applications mentioned above are commonly grown by the horizontal gradient freeze (HGF) technique. Available crystals contain large concentrations of native defects and are always p-type despite heavy compensation. These defects are mainly responsible for the unwanted absorption band from the fundamental edge near 625 nm up to 2.5 μm. The contribution of the dominant native defects to the optical absorption of $ZnGeP_2$ crystals were studied by correlating the concentration of the different centers with parts of the absorption band, by photo-EPR investigations and more directly by magnetic resonance experiments detecting magnetic circular dichroism (MCD). The corresponding results are briefly reviewed in [14].

The dominating defect in as-grown $ZnGeP_2$ is the $V_{Zn}$ acceptor [7,8], which is EPR active in the single negative charge state. The EPR spectrum shows four defect orientations, each identified by the dominant HF interaction with only two of the four surrounding P ligands (Fig. 1). Under optical activation of the samples, two compensating donors have been found. These have been attributed to the neutral phosphorus vacancy ($V_P^0$) [9] and the singly charged germanium anti-site defect ($Ge_{Zn}^+$) [10]. However, there exists no unambiguous proof for this assignment, because the large linewidth of the EPR transitions prevent the resolution of the HF interaction with the surrounding ligands. In earlier EPR studies of $ZnGeP_2$ and $CdSiP_2$ samples grown by gas phase transport, the phosphorus anti-site defect $P_{Ge}^0$ ($PP_4$-defect) on group IV site was detected [11]. This spectrum exhibits a dominating HF interaction of the unpaired spin with the central $^{31}P$ nucleus ($I$=1/2,100%, abundance) and a weaker HF interaction with all four surrounding P ligands. This defect is not discovered in HGF crystals grown under standard conditions. The germanium vacancy ($V_{Ge}$) was detected only in electron-irradiated samples

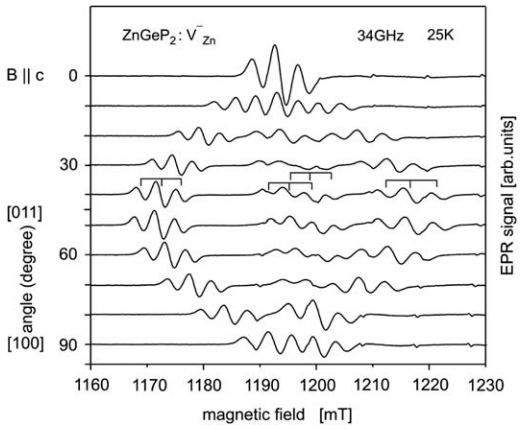


**Fig. 1.** Angular dependence of the electron transition $-1/2 \leftrightarrow +1/2$ for the four defect orientations of the negatively charged zinc vacancy $V_{Zn}^-$ in $ZnGeP_2$ by rotation of the magnetic field $B$ around the $a$-axis in the Q-band at 25 K. The two degenerated lines in the middle of the spectrum are split by a small misorientation of the $a$-axis.

[13,15]. The essential feature of this centre, which is difficult to verify in the $X$-band because of the strong overlapping with the EPR spectra caused by the zinc vacancy and the germanium anti-site, are a resolved hyperfine structure for $B \| c$ with a five-line spectrum with intensities in the ratio 1:4:6:4:1. This structure could be explained by the ligand HF interaction with four equivalent $^{31}P$ neighbors [13,15]. The recharging levels of some native defects were determined by photo-EPR [13,15,16] and optically detected magnetic resonance (ODMR) measurements [17]. It is important to emphasize that the determined energies are not the thermal ones but the optical threshold energies that differ by the Frank–Condon energy. In combination with the complementary photo-EPR investigations the ODMR measurements also reveal the contribution of the three main defects, namely the $Ge_{Zn}$ anti-site defect, the zinc and phosphorus vacancies to the broad absorption band. For a detailed consideration of the contribution of various deep native defects to the absorption and the different transitions observed in photo-EPR and ODMR, it must be taken into account that the deep levels are substantially split as a result of the low point symmetry and the anisotropy of the chemical bonding, and that the first intensive optical transition can occur from states located deep in the Brillouin zone rather than from the top of the valence band to the deep level of defects [18]. Photo-EPR and annealing experiments have shown that the commonly used reduction of the unwanted absorption by high-energy electron irradiation of the crystals is caused by recharging of the singly negative charged zinc vacancy $V_{Zn}^-$ to the diamagnetic charge state $V_{Zn}^{2-}$ [15]. EPR spectra of $ZnSiP_2$ exhibit the fingerprints of the zinc vacancy $V_{Zn}^-$, the phosphorus vacancy $V_p^0$ and the silicon anti-site $Si_{Zn}^+$ [19]. First-principle calculations of the formation energies and the energy levels in $ZnGeP_2$ were presented recently for the $V_{Zn}^-$ and the $V_{Ge}$ cation vacancies, $Zn_{Ge}$ and $Ge_{Zn}$ anti-sites [20] and for the phosphorus vacancy $V_P$ [21]. The donor ($Ge_{Zn}$) and the acceptor ($V_{Zn}$, $V_{Ge}$, $Zn_{Ge}$) character of the native defects and the position of $V_P^{+/0}$ and $Ge_{Zn}^{2+/+}$ in the band gap are in fair agreement with the experimental results obtained by photo-EPR. A close association of the dominant $V_{Zn}$ acceptor and the $Ge_{Zn}$ donor is suggested. However, there is a discrepancy between the theoretical and experimental values concerning the zinc acceptor level $V_{Zn}^{2-/-}$. While the theory [20] predicts the $V_{Zn}^{2-/-}$ charge transfer level to be 0.46 eV above the valence band, a value of 1.02 eV below the conduction band was derived from the experimental data [16]. This value is the optical threshold energy which is obtained from the photo-induced generation of the $V_{Zn}^-$ EPR spectrum for electron-irradiated samples with the Fermi level above the recharging level $V_{Zn}^{2-/-}$ [15]. Illumination of these samples with infrared light above the threshold of 1.02 eV generates simultaneously the $Ge_{Zn}^+$-related EPR signals. The observed process was interpreted as direct electron excitation from the doubly negative charged zinc vacancy ($V_{Zn}^{2-}$) to the conduction band followed by partly trapping of the photo-induced electrons in $Ge_{Zn}^{2+}$ anti-sites recharging these to the paramagnetic state $Ge_{Zn}^+$ [15]. Neglecting the Frank–Condon shift this interpretation places the $V_{Zn}^{2-/-}$ level at 1.15 eV above the VBM. The disagreement with the theoretical value is essentially removed if a direct transfer of electrons indicated from $V_{Zn}^{2-}$ to $Ge_{Zn}^{2+}$ is assumed for the observed optical quenching and activation of the EPR signals rather than a process via the valence band [20]. This possibility was primarily excluded by some reasons, because above all a much stronger photo-induced increase of the $V_{Zn}^-$ signal intensity compared to the corresponding one for $Ge_{Zn}^+$ was observed [13,15]. In addition, the photo-cross-section seems too large for a direct transfer of electrons from $V_{Zn}^{2-}$ to $Ge_{Zn}^{2+}$. However, the assumption that the 1.02 eV threshold corresponds to a direct transition from the $V_{Zn}^{2-}$ to the $Ge_{Zn}^{2+}$ level

would also explain the detected difference in the spectral dependence of the ODMR signals with the photo-EPR results [17], because the $V_{Zn}^{-}$ MCD–EPR signal interpreted as $V_{Zn}^{-} \rightarrow V_{Zn}^{0} + e_{CB}^{-}$ transition was only detected above 1.6 eV. If the theoretical predictions turn out to be true, this result suggests close association of $Ge_{Zn}$ anti-sites with $V_{Zn}$ vacancies. Another disagreement between theory and experiment is the fact that the defect wave functions of the unpaired electron of both $V_{Zn}^{-}$ and $Ge_{Zn}^{+}$ are predicted to be spread equally over the four neighboring P ions [20], whereas EPR and ENDOR data indicate only a localization, each with two of the four nearest neighboring P ions [7,8] for the four defect orientations (see e.g. Fig. 1). Very recently a Jahn–Teller distortion was discussed; this can explain the localization of the defect wave function only on two P ions [22].

Further theoretical and experimental works in combination with optical and electrical studies are necessary to finally clarify the discussed discrepancies in the level positions and the distribution of the calculated wave function. Moreover, advanced magnetic resonance experiments are required for an unambiguous identification and a detailed investigation of the properties of the native defects and defect complexes as well as to check the suggestion that some observed centers are not isolated centers but pairs or larger complexes.

We made some attempts to resolve unequivocally the nature of the dominant intrinsic defects and defect complexes in $ZnGeP_2$ with samples from different sources. An unambiguous proof, however, like for the $PP_4$-center seems only possible by resolution of additional hyperfine interactions. Though, without applying isotope-enriched Zn and Ge during the growth of $ZnGeP_2$, this can hardly be achieved due to the small natural abundance (n. a.) of Zn and Ge ions with nuclear spin ($^{67}$Zn, $I$=5/2, n. a. 4.1%; $^{73}$Ge, $I$=9/2, n. a. 7.8%).

Only one native defect EPR signal has been observed so far in $CdGeAs_2$, the material with the highest NLO coefficient, known for a phase matchable compound semiconductor [23]. The transparency range of this compound, which has a band-gap energy of about 0.57 eV (2.2 μm) at RT, extends from about 2.3 μm to beyond 17 μm. The electrical and optical properties of $CdGeAs_2$ are strongly affected by the relative concentrations of donors and acceptors unintentionally introduced during growth. The samples are usually p-type doped attributed to a shallow acceptor. Photoluminescence and optical absorption results show that most bulk $CdGeAs_2$ samples contain two distinct acceptors and one donor [24]. The shallow acceptor is located at about 0.12 eV and the deep acceptor at 0.26 eV each above the valence band maximum. The shallow donor is found at 14 meV below the conduction band [25]. The EPR signal was found to be correlated with the shallow acceptor and to have a (not well-resolved) HF splitting best simulated with two Cd and two Ge neighbors and thus identified with an acceptor on the As site. The $Ge_{As}$ anti-sites was proposed as a possible model for this shallow acceptor [26,27], rather than the alternative acceptors $V_{Cd}$ and $V_{Ge}$, but impurities such as $Si_{As}$ or $C_{As}$ could not be ruled out. Very recently, first-principle results were presented for various native defects in $CdGeAs_2$. The defect formation energies and the transition energies of the vacancies $V_{Cd}$, $V_{Ge}$, and $V_{As}$, and anti-sites $Ge_{Cd}$, $Cd_{Ge}$, $Ge_{As}$, and $As_{Ge}$ were calculated [28]. Among the three shallow acceptors ($V_{Cd}$, $Cd_{Ge}$, $Ge_{As}$) the lowest energy of formation is found for $Cd_{Ge}$, but only the $Ge_{As}$ anti-sites, which has experimentally been correlated with the observed EPR spectrum, is expected to be EPR active. No native defects identified could correlate with the experimentally observed deep acceptor and shallow donors. Therefore, it is suggested by the authors, in contrast to what is believed up to now, that both have their origins in impurities [28].

## 3. Transition metal-doped $A^{II}B^{IV}C_2^V$ semiconductors

As mentioned above, the renewed interest of the investigation of TMs in the II–IV–$V_2$ compounds arises mainly from predictions that they can exhibit charge-mediated FM above RT. These compounds were surveyed recently in a first principles calculation study [29]. In fact FM at or above RT was recently observed in some highly Mn-doped $A^{II}B^{IV}C_2^V$ semiconductors of chalcopyrite structure. These are $CdGeP_2$ [3], $ZnGeP_2$ [30,31], $ZnSnAs_2$ [32], $CdGeAs_2$ [34], and $ZnGeAs_2$ [33,35], in which a Curie temperature of $T_C$=367 K was observed [35], to date the highest $T_C$ in Mn-doped II–IV–$V_2$ compounds. FM above RT is also predicted for other TMs in these compounds [36–38], though up to now, no experimental data exist. Like in other diluted semiconductors (DMS), e.g. GaN and ZnO, the FM can be verified by the corresponding magnetization curves measured by sensitive methods like SQUID measurements. However, the microscopic mechanisms behind the FM are still unclear, because these techniques cannot differentiate between the competing exchange mechanisms in DMSs. Moreover, ferromagnetic clusters, precipitates or secondary phases embedded in the paramagnetic host lattice that are below the detection limit of X-rays diffraction (XRD) and other methods, can be responsible for the observed magnetic properties.

TM-induced FM in ternary compounds is more complex than in the binary III–V and II–VI compounds because of the two metallic sites A (group II site) and B (group IV site) that can be substituted by a TM ion. A site preference of TM ions is crucial for a potential realization of FM since substitutions on lower valence states generate donors, whereas substitutions on higher valence states generate acceptors. However, there are only a few experimental results concerning the site preference and the valence states of TMs or their interaction with native defects in these compounds [6,14,19,38]. Interesting results on Fe- and Cr-related defects in $ZnGeP_2$ were obtained very recently [6]. Moreover, incorporation of TMs into ternary compounds can locally change the free parameter $x_f$ of the chalcopyrite structure [38], which again can affect the formation of magnetic states. Another point is that FM can be caused by small undetected magnetic inclusions. For instance, the FM of Mn-doped $ZnGeP_2$ reported by Cho et al. [32] was later attributed to a MnP phase [39] on the basis of nuclear magnetic resonance (NMR) studies of similar crystals. Here, no evidence of Mn incorporated on Zn site was found [39]. However, the samples were not tested by EPR, which is more sensitive to $Mn^{2+}$. These ambivalent and incomplete results emphasize the great importance of both careful material preparation and thorough studies of the compounds applying various complementary techniques in order to distinguish between individual contributions to the observed magnetic behavior.

In the context of chalcopyrite, the DFT approach has been successfully used to explain RTFM found in Mn-doped $CdGeP_2$ taking into account intrinsic low-energy defects [5]. However, so far there has not been any experimental proof of the proposed model that assumes the incorporation of Mn on Ge site and a coupling established by holes originating from the Mn center and native defects. The formation of native defects is discussed because theoretical considerations suggest that the FM originates from the interaction of Mn centers with hole-generating native defects of the non-stoichiometric (Zn,Ge,Mn)$GeP_2$ compound [5,37].

There are only few experimental studies concerning the site preference and valence state of various TMs and their interaction with native defects in these compounds. The EPR results published until 2003 were reviewed [14]. Besides isolated $Mn^{2+}$ on group II site in II–IV–$V_2$ compounds, only the incorporation of

Fe in $CdSiP_2$ has been investigated until this time [14]. In addition, new results were published on native and Fe-related defects in $ZnSiP_2$, Mn-related defects in $ZnGeP_2$, and for the first time on anti-ferromagnetically coupled Mn–Mn pairs in $ZnGeP_2$ [14]. Later, $Cu_{Zn}^{2+}$ in $ZnGeP_2$ [40] and $Cr^{2+}$ and $Cr^{4+}$ in $CdGeAs_2$ were detected [41] and first ENDOR results on isolated $Mn^{2+}$ ions on A sites in $ZnGeP_2$ [42] and $CdGeAs_2$ [43] were published. Studies on Fe and Cr on Zn and Ge sites in $ZnGeP_2$ were done very recently [6]. The data are reviewed briefly. For very low Mn concentration, the substitution of $Mn^{2+}$ ($A^0$) on A sites was studied for $CdGeP_2$, $CdSiP_2$, $ZnSiP_2$, $ZnGeP_2$, and $ZnSiAs_2$ by EPR [11,44]. Very similar spectra were found for all investigated chalcopyrite. The spectra have axial symmetry with respect to the tetragonal axis ($c$-axis) of the lattice. According to the electron spin $S=5/2$, five fine-structure lines are detected, each being a sextet typical for the hyperfine (HF) structure of $^{55}Mn$ ($I=5/2$). The HF constant $A$ is isotropic within the experimental error and its value varies only slightly and is close to that in GaP and GaAs. This observation suggests a similar transfer of the two Mn electrons participating in the bonding to the four neighboring anions (phosphorus, arsenic) in all compounds [14]. In agreement with the observed small linewidth of the EPR signals [11,38,44] ENDOR measurements of isolated $Mn^{2+}$ ions in $ZnGeP_2$ [42] and $CdGeAs_2$ [43] reveal very small HF constants for the neighboring $^{31}P$ and $^{75}As$ nuclei indicating a strong localization of the Mn wave function. Principle values and principle-axes directions for three sets of neighboring $^{31}P$ nuclei were obtained [42]. In the case of $CdGeAs_2$ HF interaction with one set of Cd neighbors and two sets of As neighbors were measured [43]. Besides, the parameters for the Mn–HF and quadrupol interaction were determined with high precision in both cases. We note that for all investigated II–IV–$V_2$ compounds the zero-field splitting parameter $D$ for $Mn^{2+}$ has a positive sign when $Mn^{2+}$ replaces a $Cd^{2+}$ ($CdSiP_2$, $CdGeP_2$) and a negative sign when the $Mn^{2+}$ replaces a $Zn^{2+}$ ($ZnSiP_2$, $ZnGeP_2$, $ZnSiAs_2$).

There is another peculiarity concerning the formation of different magnetic states upon TM doping in II–IV–$V_2$ compounds. The incorporation of TM potentially can change the so-called free parameter $x_f$ of the chalcopyrite structure, which again may affect the formation of particular magnetic states (ferromagnetic, anti-ferromagnetic, and glass-like) [45]. Due to the spatial displacement of anions by $x_f-1/4$ from their ideal position $x_f=1/4$ for $c/2a=1$, there are always two crystallographically equivalent though magnetically nonequivalent sites each for both cations in the unit cell of ternary compounds crystallizing in the chalcopyrite structure. Both sites resulting from the clockwise and anticlockwise rotation of the anion tetrahedron around the $c$-axis by a tilting angle $\pm\tau$ can be distinguished for EPR centers with $S\geq 2$ substituted on the cation sites. Therefore, the TM-induced local change of the free parameter can be determined [11,14,38]. This was done for $Mn^{2+}$ on Zn sites in $ZnGeP_2$ [38,42] and $ZnSiP_2$ [11] as well as for $Fe^{3+}$ on $Ge^{4+}$ site in $ZnGeP_2$ [6]. The free parameter of $ZnGeP_2$ has a RT value of $x_f=0.2582$, which corresponds to a tilting angle of $\tau_{Zn}=-0.9^\circ$. The substitution of Mn on Zn site causes a strong local distortion and therefore the tilting angle increases for the $MnP_4$ unit to $|\tau_{Mn}|=5.5^\circ$ [38], $|\tau_{Mn}|=5.6^\circ$ [42]. Similar values for $\tau_{Mn}$ were obtained for Mn on Zn site in $ZnSiP_2$. While the X-ray data for the undistorted crystal yield $\tau_{Zn}=-1.9^\circ$ the Mn-induced tilting angle was determined to be $|\tau_{Mn}|=5.9^\circ$ [38]. The largest value was obtained for $Fe^{3+}$ on $Ge^{4+}$ with $|\tau_{Mn}|=7.6^\circ$ in $ZnGeP_2$ [6]. The splitting behavior is shown in Fig. 2. The changes of the free parameter $x_f$ (tilting angle $\tau$) are connected with corresponding changes of the bonding lengths and bonding angles. To determine these changes with an alternative method, extended X-ray absorption fine-structure spectroscopy (EXAFS) studies of Mn-doped $ZnGeP_2$ were done at the HASYLAB (DESY, Hamburg). The analysis of the experimental data in both the XANES (X-ray absorption near-edge spectroscopy) and EXAFS range indicate that the Mn ions substitute on cationic sites in the $ZnGeP_2$ lattice. However, it was impossible to discriminate between $Mn_{Zn}$ and $Mn_{Ge}$ sites due to similar photoelectron scattering amplitudes of Zn and Ge ions in the second coordination shell of the Mn ions. The Mn–P nearest neighbor distance was found to be 3% longer than the Zn–P bond length [46].

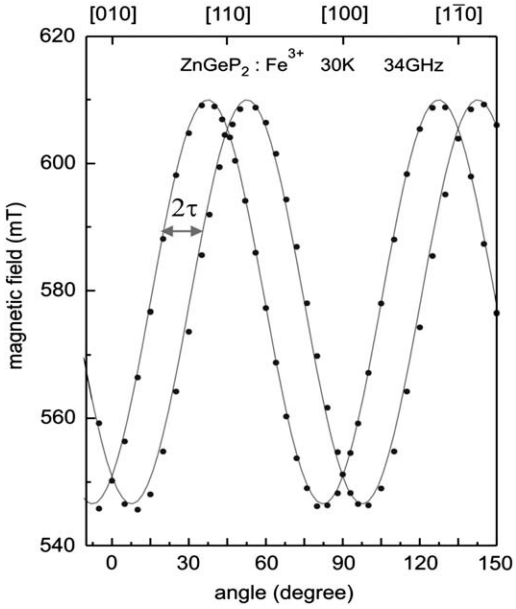


**Fig. 2.** Experimental splitting (●) of the $Fe_{Ge}^{3+}$ fine structure lines $-3/2\leftrightarrow-1/2$ for $ZnGeP_2$ by rotation of the magnetic field $B$ around the $c$-axis obtained at 34 GHz and $T=30$ K. The solid lines are calculated by exact diagonalization of the SH (1) given in [38].

Although there are several microscopic mechanisms that contribute to the zero-field splitting of $3d^5$ ions in crystals, the spin-orbit mechanism is regarded as the dominant one. There are some theoretical attempts to explain the magnitude and sign of the zero-field splitting $D$ of $d^5$ ions in different host crystals [47,48]. Assuming that the dominating contribution is given by the spin-orbit mechanism higher order perturbation formula for different symmetries were derived, which give $D$ (and also the spin-lattice coefficient $G_{11}$ and $G_{44}$) as a function of the exciting energy levels $^4P$, $^4D$, and $^4G$ relative to the $^6S$ ground state, as expressed in terms of the Racah parameter $B$ and $C$, the spin-orbit coupling constant $\xi$ and the corresponding crystal-field parameters $B_{kl}$ [47]. These parameters $B_{kl}$ are dependent on the local relaxation of the $d^5$ environment and can be expressed within the framework of the superposition model by intrinsic crystal-field parameters and functions of the angles between the impurity ligand bonding and the crystal axes [48]. For instance, from the deviation of the calculated and experimental $D$ values for $Mn^{2+}$, $Fe^{3+}$ in hexagonal GaN [49,50], and $Fe^{3+}$ in ZnO [51] a displacement of the $d^5$ ion from the corresponding cation site was calculated. In the case of the chalcopyrite with tetragonal symmetry the angle $\theta$ between the impurity ligand bonding and the tetragonal axis $c$, which describes the angular dependence of the crystal-field parameter $B_{kl}$, is linked with the free parameter $x_f$ for the group II site and for the group IV site in the host lattice by the relations [52]

$$\cos(\theta_{II})=\eta(16x_f^2+\eta^2+1)^{-1/2};$$

$$\cos(\theta_{IV})=\eta[16(x_f-1/2)^{1/2}+\eta^2+1]^{-1/2},$$

in which $\eta=c/2a$ with the lattice constants $a$ and $c$ of the chalcopyrite structure. Using these connections Zheng et al. [53–55] correlate the sign and the magnitude of the ZFS parameter $D$ and the local tilting angle $\tau$ for $Mn^{2+}$ on group II site in $ZnSiP_2$ and $CdSiP_2$ [53], $Fe^{3+}$ on $Si^{4+}$ site in $CdSiP_2$ [54] as well as very recently for $Mn^{2+}$ on group II site in $ZnGeP_2$ and $CdGeP_2$ [55]. The carried out fitting of $D$ with the local angle $\tau$ seemingly produced excellent agreement, but doubt was raised after further examinations. The reason is that in addition to the general restriction of the computation some necessary parameters for the calculation of $D$ were used that were obtained by some crude approaches as the corresponding optical data are missing. For instance, a perfect agreement between the calculated and experimental $D$ values was obtained for $ZnSiP_2$:$Mn^{2+}$ using the experimental angle $\tau_{Mn}$ and the relation between the spin-lattice coefficient $G_{11}$ and $D$ with the derived parameters [53]. However, large deviation results with the same parameters if, like in [54,55], the fourth-order perturbation formula for $D$ is employed. Moreover, it is overlooked erroneously that from the line position of the EPR transitions the sign of the tilting angle $\tau$ cannot be determined [38]. Besides, the calculations contain some numerical errors. The excellent agreement of the calculated and experimental $D$ values for $ZnGeP_2$:$Mn^{2+}$ [55] using $\tau_{Mn}=5.6^\circ$ [38,42] was obtained with a wrong local angle $\theta^{2+}_{Mn}=53.4^\circ$. Regardless of these objections, the presented approach is a first step to understand the dependence of the magnitude and sign of the zero-field splitting parameter $D$ on the TM-induced local change of the local environment. A more detailed description has to prove the validity of the formula for the calculation of the local angle $\theta_{TM}$ from the free parameter $x_f$ and include not only the nearest neighbors but also the relaxation of further ligand shells. An independent determination of the local angle $\theta_{TM}$ would be helpful for a more complete description of the local distortion. From ENDOR measurements we can obtain the orientation of the main axes for the ligands HF interaction. Unfortunately, these axes are in general not identical to the impurity ligand bonding axes.

Besides isolated $Mn^{2+}$, three other Mn-related defects have been identified in $ZnGeP_2$: a nearly isotropic Mn center with a 12% larger HF splitting, a strong axially distorted $Mn^{2+}$ center (probably caused by an associated nearest neighbor zinc vacancy) and a broad line assigned to a pair of $Mn^{2+}_{Zn}$–$Mn^{2+}_{Zn}$ ions coupled by exchange interaction [14]. The temperature dependence of the broad line shows the typical behavior of an anti-ferromagnetically exchange coupled $Mn^{2+}$–$Mn^{2+}$ pair. The temperature behavior is the result of the thermal population of the spin multiplets formed by a pair of $S_1=S_2=5/2$ spins, which are split according to the spin-Hamiltonian (SH) $\mathscr{H}=-2J_{12}S_1S_2$. For the isotropic Heisenberg exchange a value of $J_{12}\backsimeq -10\,cm^{-1}$ was obtained [14]. The formation of anti-ferromagnetically coupled $Mn^{2+}_{Zn}$–$Mn^{2+}_{Zn}$ pairs was confirmed by the detection of the different transitions within the spin multiples having total spins $S=1, 2, 3, 4, 5$ and their characteristic hyperfine structure in high-quality Mn-doped $ZnGeP_2$ crystals that is produced by the interaction of two $^{55}Mn$ nuclei with $I=5/2$ [6]. The characteristic HF splitting in 11 hyperfine lines with the intensity ratio 1:2:3:4:5:6:5:4:3:2:1 and the half hyperfine splitting observed for isolated $Mn^{2+}$ on Zn site is shown in Fig. 3.

Systematic ab-initio calculations of the energy difference between ferromagnetic and anti-ferromagnetic spin arrangements of near neighbor Mn ions are used to investigate the magnetic properties of doped $CdGeP_2$, $ZnGeP_2$, $ZnGeAs_2$, $ZnSnP_2$, and $ZnSnAs_2$ [56]. While for $Mn_{II}$–$Mn_{II}$ pairs a strong preference for anti-ferromagnetic interactions is predicted, the other pairings $Mn_{II}$–$Mn_{IV}$ and $Mn_{IV}$–$Mn_{IV}$ are ferromagnetic for all compounds except $CdGeP_2$ [56]. Similar results were obtained for Mn-doped

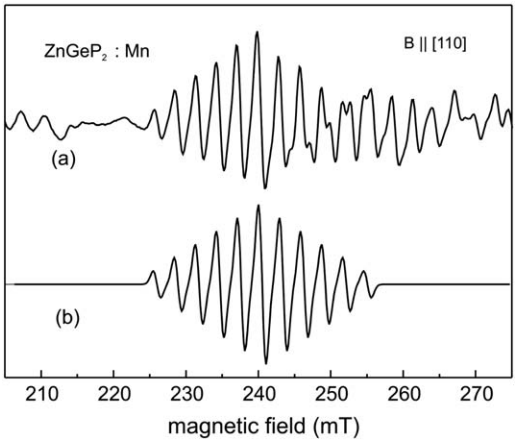


**Fig. 3.** Resolved HF interaction for the $Mn^{2+}_{Zn}$-$Mn^{2+}_{Zn}$ pairs in $ZnGeP_2$ for $B\|[1\,1\,0]$ at 5 K for the transition $-1\leftrightarrow 0$ of the spin state $S=1$, which is partly overlapped with a transition within the spin state $S=2$ (a). For the simulated structure (b), the half HF splitting of the isolated $Mn^{2+}_{Zn}$ of $A=-52.8\times10^{-4}\,cm^{-1}$ and the characteristic intensity ratio 1:2:3:4:5:6:5:4:3:2:1 of the 11 lines of such pair were used (after [6]).

$ZnGeP_2$ and $ZnGeAs_2$, whereas $Cr_{II}$-$Cr_{II}$ pairs show in agreement with [36] ferromagnetic behavior [57].

In addition to the described Mn and Fe defects [6,14,38] in $ZnGeP_2$ with tetragonal symmetry, we also observed weak Mn and Fe resonances, which are associated with defects of lower symmetry, probably in conjunction with native defects. However, the strong overlap of the different Mn-induced EPR spectra and the overlap of the various complicated Fe spectra together with the low intensity of the low-symmetry spectra have so far prevented a complete analysis.

In a recent EPR study on exchange interactions of Mn ions in $CdGeAs_2$ doped with 6% Mn, two types of Mn ions were discussed occupying the Cd site ($Mn^{2+}_{Cd}$) and the $Ge^{4+}$ site ($Mn_{Ge}$). According to the given interpretation they form $Mn^{2+}$ ($S=5/2$) complexes with two heavy holes ($S=3/2$ each) of the valence band with a resulting spin $S=1/2$ [58]. In fact, no evidence was found in the doped bulk crystals suggesting $Mn^{4+}$ substitution on $Ge^{4+}$ site. In contrast, EPR and ENDOR investigations by Evans et al. [43] showed no evidence suggesting that $Mn^{4+}$ ions substitute for $Ge^{4+}$ in bulk crystals with a $Mn^{2+}$ concentration up to $9\times10^{20}\,cm^{-3}$.

Furthermore, there are more four EPR papers on Mn-doped $ZnGeP_2$ [59–62]. The authors studied (Zn,Mn)$GeP_2$ layers grown on $ZnGeP_2$ substrate by solid-phase reactions at 400–550 °C. Mn was introduced by means of in-diffusion. Weak EPR resonances originating from $Mn^{2+}$ in the bulk proved that Mn had diffused into the bulk material [59,60]. A broad line was detected up to room temperature that was designated tentatively to FMR in the (Zn,Mn)$GeP_2$ layer [59]. A Curie temperature of $T_C=318$ K was determined from the temperature dependence of the magnetization observed by SQUID measurements [60]. On the basis of obvious differences between the spectra of $ZnGeP_2$ samples with nominal Mn concentrations of 0.2% and 2%, the authors drew the conclusion of the detection of two types of isolated Mn centers without thorough analysis. There are no reasons why the "new" spectrum described should be caused by $Mn^{2+}_{Ge}$ ($A^{2-}$) with $S=5/2$ from a $^6A_1$ ground state or $Mn^{3+}_{Ge}$ ($A^-$) from a $^5T_2$ ($^5D$) with $S=2$. Indeed, the appearance of isolated Mn in different charge states on Ge site is in accordance with theoretical predictions [5]. However, the mentioned differences are well-known and in agreement with a concentration-dependent broadening of the fine-structure lines (see, e.g. [49]). No details are given concerning the additionally

observed broad resonance which supposedly shows an anomalously intense dispersion signal. In fact, the presented dispersion signal exhibits the normal behavior which is detected for a slightly saturated absorption signals. In summary, these four papers [59–62] claim to present results that corroborate theoretical predictions. However, under closer investigation those results turn out to be inconclusive. Lacking a quantitative analysis, the observed EPR spectra seem to be interpreted in an incorrect way.

Whereas the incorporation of $Fe^{4+}$ [63] and $Cr^{4+}$ [41] on group IV site of $CdSiP_2$ and $CdGeAs_2$, respectively, has been well-known for quite a while, the substitution of $3d^n$ ions in $ZnGeP_2$ on group IV site had not been reported until very recently [6]. Simultaneous doping of $ZnGeP_2$ by low concentrations of Fe and Cr during the HGF growth process, results in substitution of $Ge^{4+}$ by $Fe^{3+}$ ($B^-$) and $Cr^{4+}$ ($B^0$) as well as of $Zn^{2+}$ by $Fe^{2+}$ ($A^0$). A photo-induced recharging of $Fe^{2+}$ ($3d^6$, $^5D$, $S=2$) to $Fe^+$ ($3d^7$, $^4A_2$, $S=3/2$) is observed. This shows that the negatively charged acceptor state $Fe^+(A^-)$ sits closely below the CB within the band gap similar to the one in $ZnSiP_2$ [19], where this defect can be observed without illumination as the samples are n-type. This makes the discussed alloys to be potential candidates for electron-mediated FM. The $Cr^{4+}$ ($3d^2$, $^3A_2$, $S=1$) center exhibits a well-resolved phosphorus ligand hyperfine splitting, revealing a significant delocalization of the unpaired spin which is a good condition for hole-mediated FM. However, neither in low-doped $CdGeAs_2$:Cr [41] nor $ZnGeP_2$:Cr [6] the theoretical predicted FM [36,57] was detected.

The observed site preference of the TM regarding the group II and group IV sites depending on its charge state is crucial for a possible explanation of FM since substitution on lower valence states generates donors, whereas substitution on higher valence states generates acceptors. Therefore, only the substitution of the negatively charged acceptor $Fe^{3+}_{Ge}(B^-)$ for the higher valence states $Ge^{4+}$ is desirable due to releasing of charge carriers (holes), a precondition for hole-mediated FM.

## 4. Summary and outlook

The present article discusses the identification of native defects in II–IV–$V_2$ compounds by magnetic resonance methods (EPR, photo-EPR, ENDOR, ODMR). Data are only available for $ZnGeP_2$, $ZnSiP_2$, and $CdGeAs_2$ The dominant native defects in $ZnGeP_2$ and $ZnSiP_2$ are the zinc ($V_{Zn}$) and phosphorus ($V_P$) vacancy as well as the group IV anti-site defect $Ge_{Zn}(Si_{Zn})$, which are also mainly responsible for the observed optical absorption extended from the fundamental edge up to 2.5 μm. In addition, the Ge vacancy ($V_{Ge}$) is observed in electron-irradiated $ZnGeP_2$ samples and the phosphorus anti-site defect $P_{Ge}$ ($PP_4$ defect) in $ZnGeP_2$ and $CdSiP_2$ grown by gas phase transport. The energy level positions of the observed native defects in $ZnGeP_2$ are determined by photo-EPR and MCD-EPR measurements. Good agreement is obtained with theoretical predictions based on density functional theory. The theoretical studies suggest a close association between the dominant acceptors ($V_{Zn}$) and donors ($Ge_{Zn}$). But there is up to now no evidence that some of the observed isolated defects are in truth pair defects or complexes. The use of samples that are grown under other conditions and the use of samples with isotopically enriched cation isotopes should be helpful in order to resolve unequivocally the nature of the native defects and to detect some of the up to now unobserved anti-sites defects. Only one native defect, which is correlated with a shallow acceptor, was found by EPR for $CdGeAs_2$. This defect is tentatively identified as $Ge_{As}$ anti-sites.

Comprehensive insights into the role of TMs for the formation of FM in $A^{II}B^{IV}C^{V}_2$ compounds can be achieved by detailed studies of their site preference, geometric configurations and valance states in dependence on doping concentration and Fermi level. However, up to now there are apart from Mn only a few data for other TM (Cu, Fe, Cr) ions. At low concentrations, Mn is incorporated into $ZnGeP_2$ as isolated $Mn^{2+}$ on the two magnetically nonequivalent $Zn^{2+}$ sites. The Mn substitution on Zn site causes a strong local distortion of the free parameter $x_f$, which describes the positions of the anions in the chalcopyrite structure. At higher Mn concentrations, additional resonances show up in the EPR spectrum. Their origins are a nearly isotropic Mn defect with larger HF interaction, a Mn defect of monoclinic symmetry, and $Mn^{2+}_{Zn}$–$Mn^{2+}_{Zn}$ pairs. Possible signals originating from $Mn^{3+}(B^-)$ and $Mn^{4+}(B^0)$ on $Ge^{4+}$ site and their interaction with native defects are hard to detect due to the strong overlapping of the different Mn spectra and with the EPR signals from native defects.

According to the existing theoretical predictions only the incorporation on group IV sites or the interaction of TMs with native defects should result in charge-mediated FM. Direct evidence for the incorporation of TM on group IV site could be obtained up to now only for $CdSiP_2$: $Fe^{4+}(B^0)$, $CdGeAs_2$: $Cr^{4+}$ ($B^0$), $ZnGeP_2$: $Fe^{3+}$ ($B^-$) and $ZnGeP_2$: $Cr^{4+}(B^0)$ for low doping concentrations. In all cases no FM was detected. But, neither the interaction with native defects nor the doping behaviors for higher concentrations and for different Fermi levels were investigated. Consolidated findings on the role of TMs by the generation of FM in II–IV–$V_2$ compounds can be expected by detailed and systematic studies of their site preference as a function of their concentration and the position of the Fermi level as well as the study of the pair and small cluster formation for higher doping concentrations.

## Acknowledgements

The authors are indebted to N. Dietz, V.G. Voevodin, O.V. Voevodina, G.A. Verozubova, and S. Unterricker for providing undoped and TM doped $ZnGeP_2$ and $ZnSiP_2$ crystals. We are greatly indebted to R.N. Pereira and D. Azamat for their essential contributions to the presented photo-EPR and EPR results.

## References

[1] N. Dietz, et al., Mater. Sci. Eng. B 97 (2003) 182.
[2] E. Lippert, et al., Opt. Express 16 (2008) 13878.
[3] G.A. Medvedkin, et al., J. Appl. Phys. 39 (2000) L949.
[4] S. Cho, et al., Phys. Rev. Lett. 88 (2002) 257203.
[5] P. Mahadevan, et al., Phys. Rev. Lett. 88 (2002) 47205.
[6] W. Gehlhoff, et al., Physica B 376–377 (2006) 790.
[7] L.E. Hulliburton, et al., Appl. Phys. Lett. 66 (1995) 2670.
[8] K.T. Stevens, et al., MRS Symp. Proc. 484 (1998) 549.
[9] N.C. Giles, et al., Appl. Phys. Lett. 66 (1995) 1758.
[10] N.C. Giles, et al., J. Appl. Phys. 93 (2003) 8975.
[11] U. Kaufmann, et al., Phys. Status Solidi (b) 74 (1976) 169.
[12] S.D. Setzler, et al., Appl. Phys. Lett. 74 (1999) 1218.
[13] W. Gehlhoff, et al., Phys. Status Solidi (b) 235 (2003) 151.
[14] W. Gehlhoff, et al., Mater. Sci. Semicond. Process. 6 (2003) 379.
[15] W. Gehlhoff, et al., J. Phys. Chem. Solids 64 (2003) 1923.
[16] W. Gehlhoff, et al., Physica B 308–310 (2001) 1015.
[17] D.M. Hofmann, et al., Physica B 340–342 (2003) 978.
[18] V.N. Brudnyi, et al., Phys. Solid State 48 (2006) 2069.
[19] W. Gehlhoff, et al., Physica B 340–342 (2003) 933.
[20] X. Jiang, et al., Phys. Rev. B 71 (2005) 205212.
[21] X. Jiang, et al., Phys. Rev. B 73 (2006) 193203.
[22] X. Jiang, et al., Chin. Phys. Lett. 25 (2008) 1075.
[23] M.C. Ohmer, et al., Mater. Res. Bull. 23 (1998) 16.
[24] L. Bai, et al., J. Appl. Phys. 97 (2005) 023105.
[25] L. Bai, et al., J. Appl. Phys. 95 (2004) 4840.
[26] L.E. Halliburton, et al., J. Appl. Phys. 77 (1995) 435.
[27] L. Bai, et al., Mater. Res. Soc. Symp. Proc. 744 (2003) 537.
[28] T.R. Paudel, et al., Phys. Rev. B 78 (2008) 085214.
[29] S.C. Erwin, I. Zutic, Nat. Mater. 3 (2004) 410.
[30] S. Choi, et al., Solid State Commun. 122 (2002) 165.

[31] G.A. Medvedkin, et al., J. Cryst. Growth 236 (2002) 609.
[32] S. Cho, et al., Phys. Rev. Lett. 88 (2002) 257203.
[33] S. Choi, et al., J. Korean Phys. Soc. 42 (2003) S739.
[34] R. Demin, et al., Phys. Status Solidi (c) 1 (2004) 3525.
[35] L.I. Koroleva, et al., Phys. Solid State 49 (2007) 2121.
[36] T. Kamatani, H. Akai, Phase Transit. 76 (2003) 401;
T. Kamatani, H. Akai, Mater. Sci. Semicond. Process. 6 (2003) 389.
[37] Hongsuk Yi, et al., Physica B 359–361 (2005) 1466.
[38] W. Gehlhoff, et al., Phys. Status Solidi (b) 242 (2005) R14.
[39] T. Hwang, et al., Appl. Phys. Lett. 83 (2003) 1809.
[40] K.T. Stevens, et al., J. Phys.: Condens. Matter 15 (2003) 1625.
[41] N.Y. Garces, et al., J. Appl. Phys. 94 (2003) 7567.
[42] N.Y. Garces, et al., Phys. Rev. B 72 (2005) 033202.
[43] S.M. Evans, et al., Phys. Status Solidi (b) 243 (2006) 4070.
[44] N.P. Baran, et al., Sov. Phys. Semicond. 9 (1976) 1527.
[45] Y.J. Zhao, et al., Phys. Rev. B 65 (2002) 94415.
[46] R. Bacewicz, et al., Phys. Status Solidi (a) 204 (2007) 2296.
[47] W.L. Yu, M.G. Zhao, Phys. Rev. B 37 (1988) 9254.
[48] D.J. Newman, et al., Rep. Prog. Phys. 52 (1989) 699.
[49] T. Graf, et al., Phys. Rev. B 67 (2003) 165215.
[50] W.-C. Zheng, J. Zi, et al., Z. Naturforsch. A Phys. Sci. 56 (2001) 473.
[51] Li Ju-Feng, et al., Chem. Phys. Lett. 429 (2006) 266.
[52] J.E. Jaffer, A. Zunger, Phys. Rev. B 29 (1984) 1882.
[53] W.-C. Zheng, et al., Physica B 315 (2002) 223.
[54] W.C. Zheng, et al., Spectrochim. Acta A 58 (2002) 1779.
[55] L. Hong-Gang, et al., Spectrochim. Acta A 71 (2008) 417.
[56] P.R.C. Kent, et al., AIP Conf. Proc. 772 (2005) 1369.
[57] A.V. Krivosheeva, et al., in: V.E. Borisenko, S.V. Gaponenko, V.S. Gurin (Eds.), Physics, Chemistry and Application of Nanostructures, Springer, 2007, pp. 66–69.
[58] S.V. Gudenko, et al., JETP Lett. 82 (2005) 532.
[59] G.A. Medvedkin, et al., Phys. Chem. Sol. 64 (2003).
[60] P.G. Baranov, et al., J. Supercond. 16 (2003) 131.
[61] P.G. Baranov, et al., JETP Lett. 77 (2003) 582.
[62] P.G. Baranov, et al., Physica B 340–342 (2003) 878.
[63] U. Kaufmann, Phys. Rev. B 14 (1976) 1848.